Available online at www.sciencedirect.com
SCIENCE DIRECT
Journal of Catalysis 240 (2006) 137–150
JOURNAL OF CATALYSIS
www.elsevier.com/locate/jcat

Pt/C stabilization for catalytic wet-air oxidation: Use of grafted TiO_2

Cheng-Chieh Shih, Jen-Ray Chang *

Center for Nanotechnology Design & Prototyping, Department of Chemical Engineering, National Chung Cheng University, Chia-Yi, Taiwan, ROC

Received 25 December 2005; revised 14 March 2006; accepted 22 March 2006

Available online 24 April 2006

Abstract

The wet-air oxidation (WAO) process is effective in converting organic pollutants in wastewater to innocuous carbon dioxide. Supported Pt catalysts, particularly Pt/C, are effective but unstable. A novel catalyst, Pt on TiO_2-grafted carbon (Pt/TiO_2-C), has been developed for WAO. This catalyst is characterized by high activity and stability in WAO processes. Using transmission electron microscopy (TEM), extended X-ray absorption fine structure (EXAFS), and Fourier transform infrared (FTIR) spectroscopy, the fresh and aged Pt/C catalysts were characterized, and the mechanism of catalyst deactivation was elucidated. The average Pt cluster size increased from about 2 to 10 nm after WAO of methanol in water at 220 °C for 200 h. These results indicate that Pt/C catalyst was deactivated due to migration and aggregation of the Pt clusters into large Pt particles. The increase in the content of oxygen-containing groups and carbonate species, as characterized by FTIR spectra in the aged catalyst, further suggests that the oxidation of carbon surface decreases the affinity between Pt and the carbon support, leading to extensive Pt aggregation. Thus, TiO_2 was grafted on to the carbon support to anchor and keep Pt from migrating and agglomerating, thereby obtaining a stable Pt/TiO_2-C catalyst. The efficacy of TiO_2 grafted on activated carbon in stabilizing the Pt/C catalyst was demonstrated in long-term catalytic performance tests. The efficacy of TiO_2 in anchoring and maintaining the Pt clusters in small ensembles were further demonstrated by characterizing the Pt–TiO_2 interactions and the morphology of Pt clusters using EXAFS.

Keywords: Grafted TiO_2; Extended X-ray absorption fine structure; Carbon-supported Pt catalysts; FTIR spectroscopy; Wet-air oxidation; Catalyst deactivation

1. Introduction

Wastewater effluents from chemical or petrochemical plants are often contaminated with a wide range of organic pollutants. In general, these pollutants are too toxic for conventional biological treatments, such as active sludge treatment, and too dilute to treat by direct incineration. Wet-air oxidation (WAO) is an effective way to destruct such organic contaminants in industrial wastewater. WAO has been thoroughly reviewed by various authors, including Mishra et al. [1], Levec et al. [2], Luck [3,4], and Imamura [5]. WAO can be either a catalytic or a noncatalytic operation. A typical noncatalytic WAO process is operated at elevated temperatures and pressures, making application of this technology economically unattractive. However, WAO can be greatly improved by using catalysts. Catalytic WAO can be operated under conditions much milder than those required by noncatalytic WAO, leading to significant savings in both equipment and operation costs.

Currently the most commonly used heterogeneous catalysts in WAO are transition metal oxides or noble metals (Pt, Pd) supported on nonreducible metal oxides, such as alumina, silica, and zeolite. However, these inorganic supports can be dissolved slowly in the hot acidic wastewater streams during extended operation. Hydrophobic catalysts, such as styrene–divinyl benzene copolymer (SDB)-supported noble metal catalysts, are active for WAO, but under the oxidative environment, the metals can be leached out and the supports can crumble, leading to rapid catalyst deactivation [6].

Activated carbons have long been used as catalyst supports in the fine chemical industry because of their high surface area, rapid adsorption kinetics, and high acidic and basic resistance [7]. In recent years, transition metals on activated carbon have been demonstrated to be effective for catalytic WAO of

* Corresponding author. Fax: +886 5 2721206.
E-mail address: chmjrc@ccu.edu.tw (J.-R. Chang).

0021-9517/$ – see front matter
doi:10.1016/j.jcat.2006.03.019

organic acid-containing wastewater [8–11]. However, the carbon support can be catalytically combusted around the metal sites during the oxidation of organic compounds in wastewater [12,13]. The carbon combustion causes destruction of the pore structure and development of surface oxygen-containing groups of activated carbon [14], leading to catalyst deactivation.

The goal of this study was to develop an activated carbon-supported Pt catalyst that is active and stable for WAO of wastewater. The effects of reaction temperature on the structure and catalytic stability of Pt/C catalysts were investigated, and the mechanism of its deactivation was elucidated. Based on the deactivation mechanism, a Pt/C that is stable for WAO was developed. In catalyst preparation, Pt was anchored on the carbon support grafted with TiO_2, leading to a Pt/TiO_2-C catalyst. The efficacy of this catalyst was demonstrated based on long-term catalytic performance data. The mechanism of catalyst stabilization using grafted TiO_2 was elucidated using extended X-ray absorption fine structure (EXAFS) characterization and Fourier transform infrared (FTIR) techniques.

Tryba et al. reported the preparation of TiO_2-mounted activated carbon, which was found to be effective in removing phenol from water under ultraviolet irradiation [15]. According to X-ray diffraction (XRD), the TiO_2 particles were well-crystallized anatase with sizes of few μm. Preparation of highly dispersed TiO_2 on nonreducible metal oxide supports such as silica and MCM-41 has been reported by Srinivasan et al. [16] and Lin et al. [17], respectively. The grafted TiO_2 on nonreducible metal oxides has been prepared by reaction of surface hydroxyl groups on the metal oxides with titanium precursors like titanium alkoxides, followed by drying and calcinations [16–19]. Thus, the same approach was used to graft TiO_2 on activated carbon to anchor the Pt clusters. Phenolic hydroxyl groups on activated carbon can react with Ti alkoxides to produce Ti–O–C linkage with elimination of one alcohol and make Ti immobile. However, the activated carbon should be dried before the grafting procedure to remove absorbed water on its surface such that hydrolysis of metal alkoxides in the latter grafting step can be avoided. In addition, the grafting reaction should be carried out under inert environment to avoid the hydrolysis of metal alkoxides.

In this study, a continuous fixed-bed reactor working in a trickle-flow regime was used to characterize the catalytic properties and performance of the catalyst for WAO. Pure water containing methanol was used as the model wastewater to decouple other effects, such as inorganic compounds on the catalytic performance. Transmission electron microscopy (TEM) and EXAFS spectroscopy were used to characterize the catalyst structure, and FTIR spectroscopy was used to characterize functional groups of the carbon supports.

2. Experimental

2.1. Materials and catalyst preparation

Activated carbon (GAC 830, from Norit, in granular form with surface area, 1050 m^2/g; pore volume, 0.85 mL/g; iodine no. 75 mg/g minimum; diameter 1.5 mm; and apparent density, 0.54 g/mL) was brought into contact with a solution of $Pt(NH_3)_4(NO_3)_2$ (Strem, 99.9%) in doubly distilled deionized water. The amount of Pt precursor was chosen so that on adsorption of the entire Pt, the catalyst would contain 1.0 wt% Pt. After impregnation, the resulting material was evacuated at 10^{-2}–10^{-3} Torr and 60 °C for 2 h. The sample was noted as $[Pt(NH_3)_4(NO_3)_2]$/C.

A total of 10 g of the activated carbon was evacuated at 10^{-2}–10^{-3} Torr and 120 °C for 24 h to remove the adsorbed water. The dried activated carbon was then placed in a flask with side arm under nitrogen. Then 10 g of titanium(IV) ethoxide ($Ti(OC_2H_5)_4$ (Acros) was dissolved in 10 mL of absolute ethanol and then added into the flask. This mixture was stirred overnight and then evacuated at 10^{-2}–10^{-3} Torr and about 60 °C for 2 h. The resulting powder was pretreated at 200 °C for 2 h under air and finally calcined at 600 °C for 4 h under nitrogen. The sample was noted as TiO_2-C. Compared with the original activated carbon, the surface area of TiO_2-C decreased from 1050 to 720 m^2/g and the average pore diameter decreased from 2.63 to 2.15 nm, whereas no crystalline TiO_2 peaks have been detected by powder synchrotron XRD at a wavelength of 1.070 Å.

The preparation procedures and conditions for Pt/C were applied to prepare TiO_2-C-supported Pt catalysts. The resulting catalyst sample was denoted as Pt/TiO_2-C.

2.2. Catalytic performance

The catalytic performance tests for Pt/C were conducted in a continuous-downflow fixed-bed reactor. The reactor was a stainless-steel tube with an inside diameter of 2.1 cm and volume of 94.0 mL. It was heated electrically and controlled by a PID temperature controller with a sensor in the center of the catalyst bed. Then 1 g of the catalyst sample $[Pt(NH_3)_4(NO_3)_2]$/C] was mixed with inert ceramic of 0.2 cm at a ratio of 1 to 5, and the top of the reactor bed was filled with 1.6-mm glass balls to preheat and prevent channeling of the feed. Using this packing method, the porosity of the catalyst bed was about 0.35. The samples were converted to Pt/C by predrying in flowing N_2 at 200 °C and then reducing in flowing H_2 at 300 ± 10 °C for 2 h before reaction. Pure water containing 0.25 wt% methanol was used as the model wastewater for the aging test. The reaction was carried out at an airflow rate so as to maintain an O_2-to-methanol molar ratio of 75. The reduced Pt/C samples were tested at WHSV of 6 h^{-1} of four different temperature and pressure conditions: 130 ± 10 °C and 5 atm, 160 ± 10 °C and 10 atm, 180 ± 10 °C and 20 atm, and 220 ± 10 °C and 40 atm; the corresponding used catalysts were denoted as T130P5W6, T160P10W6, T180P20W6, and T220P40W6, respectively. To keep the reaction in a trickle-flow regime, the pressures were increased with reaction temperatures. The reaction products were trapped using a condenser at −5 °C and analyzed using a gas chromatography (Shimadzu model GC-14A, with a thermal conductivity detector, a DB-WAX capillary column, and a SP4270 data processor). After the test reactions, the catalysts were purged with nitrogen to remove adsorbed oxygen and wa-

ter, then unloaded from the reactor in nitrogen environment for characterization.

To compare the stability of the Pt/C and Pt/TiO_2-C catalysts, the same procedures for catalyst pretreatment, catalyst packing, and product analysis were applied for these two catalysts, whereas the reaction was carried out at 220 ± 10 °C, 40 atm, and a WHSV of 24 h^{-1}. The used catalyst for the Pt/C and Pt/TiO_2-C catalysts were denoted as T220P40W24 and T220P40W24(Pt/TiO_2-C), respectively.

2.3. FTIR spectroscopy

Fresh and used Pt/C and Pt/TiO_2-C samples were characterized by use of FTIR spectroscopy using a Shimadzu FT-IR 8101M with a spectral resolution of 2 cm^{-1} and equipped with a SSU-8000 second sampling unit. The wafers (4 wt% $[Pt(NH_3)_4(NO_3)_2]$/C or $[Pt(NH_3)_4(NO_3)_2]$/TiO_2-C sample in KBr) were loaded into an IR cell in an N_2-filled glove box. The samples were predried and reduced at the same conditions as used for catalytic performance tests. After the treatments, IR spectra were recorded. For the used catalyst samples, the samples were purged with N_2 at room temperature to remove adsorbed species before IR spectrum measurement.

2.4. X-ray absorption spectroscopy

The X-ray absorption measurements were performed on the wiggler beamline BL17C at National Synchrotron Radiation Research Center (NSRRC), Taiwan. The electron storage ring was operated at an energy level of 1.5 GeV and a beam current of 120–200 mA. A Si(111) double-crystal monochromator was used for energy selection, and mirrors rejected higher harmonic radiation. The transmission geometry was arranged using gas-filled ionization chambers to monitor the intensities of the incident and transmitted X-ray beams. A full spectrum for Pt L_{III} absorption edge (11564 eV) was obtained over the energy level of 11364–12764 eV. Similarly, a full spectrum for Ti K edge (4966 eV) was obtained at 4766–5966 eV. The fresh and used catalyst samples were loaded into an EXAFS cell in an N_2-filled glove bag. For the used catalyst samples, the EXAFS measurements were performed after an N_2 purge at room temperature. For the fresh catalyst samples, the samples were reduced in an EXAFS cell using the same operating conditions as used in the catalytic performance tests. A standard Pt foil at room temperature was simultaneously measured as a reference so that energy calibration could be done between scans.

Appropriate reference data are necessary for detailed analysis of EXAFS data characterizing the catalyst samples. The EXAFS contributions for Pt–Pt, Pt–O, and Ti–Ti were analyzed with phase shifts and backscattering amplitudes obtained from EXAFS data for Pt foil, $Na_2Pt(OH)_6$, and Ti foil, respectively. The Ti–O, Ti–Pt, and Pt–Ti were analyzed with phase shifts and backscattering amplitudes calculated from FEFF.

2.5. TEM

The fresh and used Pt/C and Pt/TiO_2-C samples were carefully pulverized, dispersed in ethanol, fetched on Cu grids, and then dried for later TEM analysis. The TEM (Philips, TECNAI 20) is typically operated at 200 keV.

2.6. CO chemisorption

A quartz tube was packed with catalyst sample of about 0.2 g. After pretreatments and hydrogen reduction, consecutive 0.1-mL pulses of CO were injected into catalyst bed with He as the carrier gas until no more CO uptake was detected. The amount of chemisorption was then calculated by summing up the proportions of all pulses consumed.

3. Results and discussion

3.1. Catalytic performance of Pt/C and Pt/TiO_2-C in WAO of methanol

In the WAO process, essentially, the entire methanol is converted to CO_2 as shown in the following equation:

$$CH_3OH + (3/2)O_2 \rightarrow CO_2 + 2H_2O.$$

Because of the high conversion levels, methanol oxidation in WAO can be considered a total oxidation.

For Pt/C catalyst, the activity is high but the stability becomes poor at higher temperatures. The conversion of methanol in the model wastewater as a function of time on stream at a temperature range of 130–220 °C is shown in Fig. 1. The Fig. 1 shows that the initial catalyst activity was high and total oxidation of methanol was achieved, consistent with the work of Cheng et al. [20]. However, in the aging test for an extended operational period, the catalyst activity was maintained only at reaction temperatures below 160 °C and decreased gradually at reaction temperatures above 180 °C. These results indicate that

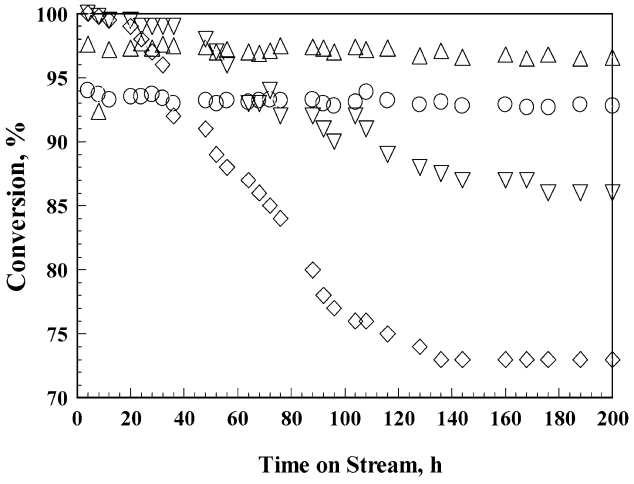

Fig. 1. Methanol conversion at WHSV = 6 h^{-1} as a function of time on stream in aging test: (○) 130 °C and 5 atm; (△) 160 °C and 10 atm; (▽) 180 °C and 20 atm; (◇) 220 °C and 40 atm.

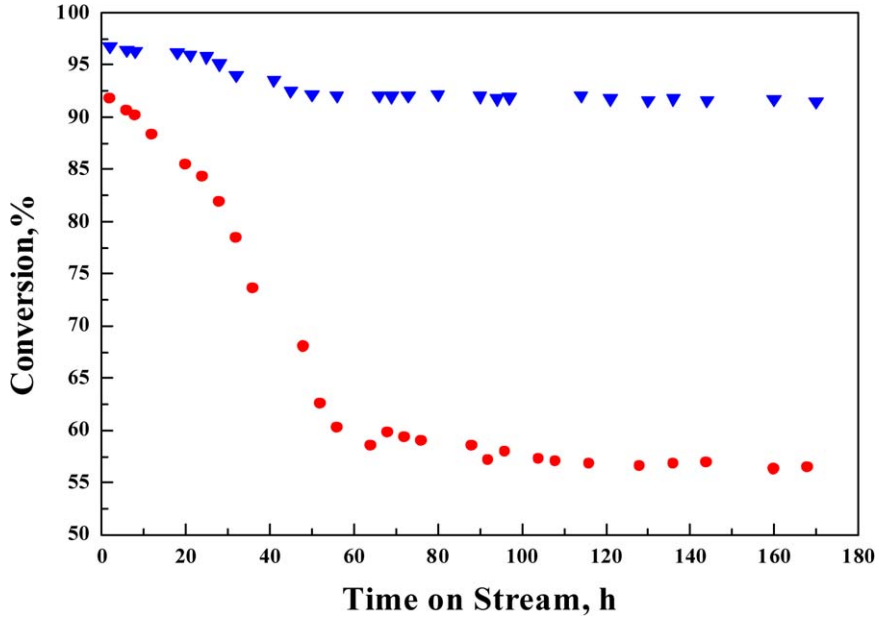

Fig. 2. Comparison of methanol conversion for different catalysts at 220 °C, 40 atm, and WHSV = 24 h^{-1} as a function of time on stream in aging test: (○) Pt/C; (▽) Pt/TiO_2-C.

Pt/C catalysts are stable at lower reaction temperatures (say, below 160 °C), but deactivated at 180 °C or higher.

Methanol conversion is shown as a function of time on stream in the flow reactor at WHSV of 24 h^{-1}, 220 °C, and 40 atm for Pt/C and Pt/TiO_2-C catalysts (Fig. 2). The initial conversion of methanol for the Pt/TiO_2-C catalyst sample was higher than that for the Pt/C catalyst, with a conversion of 97 and 92%, respectively. Whereas the conversion for Pt/TiO_2-C remained rather constant, that for Pt/C fell sharply with time on stream.

The external mass transfer limitation was examined by the methanol conversion over the Pt/C catalysts, carried out at a constant WHSV (24 h^{-1}) with variable superficial mass flow velocities, u_s, ranging from 2 to 40 g/(cm^2 h); where u_s = (mass flow rate, g/h)/(inside cross-section of the reactor, cm^2) (porosity of catalyst bed). The experimental results indicated that methanol conversion increased with increasing superficial velocity; the methanol conversions were 0.46, 0.76, 0.92, 0.94, and 0.95 for superficial mass velocities of 4, 10, 20, 40, and 80 g/(cm^2 h), respectively. In addition, when the catalyst was pulverized from 1.5 mm to about 0.1 mm, the conversion increased from 0.92 to 0.96 for the superficial mass velocity of 20 g/(cm^2 h). These results suggested that the tests for comparing the stability of the Pt/C and Pt/TiO_2-C catalysts operated in the regimes of combined chemical reaction and mass transfer control.

Because the purpose of this paper is to investigate the role of the grafted TiO_2 in improving the catalytic properties of Pt/C catalysts, rigorous kinetic analysis was not attempted. As shown below, an empirical power law rate equation and overall effectiveness factor are adequate to explain qualitatively that the improvement in catalytic properties was attributable to the use of grafted TiO_2 in this study.

For the Pt/C catalyst, at the start of runs, the methanol conversions were 0.76, 0.86, 0.92, and 0.95 for WHSV of 48, 32, 24, and 16 h^{-1}, respectively. These data could be roughly fitted by first-order kinetics with an observed rate constant of 36 h^{-1}. Thus, the reaction rate can be formulated as $r_{obs} = \eta_o k_v C_b = k_o C_b$, where r_{obs} is the observed reaction rate, k_o is the observed rate constant, k_v is the intrinsic rate constant, C_b is the concentration of methanol, and η_o is the global effectiveness factor. Because both internal and external mass resistance are involved in the reaction system, overall mass transfer resistance is formulated as $1/\eta_o = \varphi/\tanh\varphi + k_v/k_e(V_p/S_x)$ and $\varphi = R(k_v/D_e)^{0.5}$, where k_e is the external mass transfer coefficient, V_p is the volume of a catalyst pellet, S_x is the external surface area of a catalyst pellet, D_e is the effective diffusivity, and R is the radius of a catalyst pellet [21]. In testing Pt/C and Pt/TiO_2-C catalysts, the geometry of the catalyst pellets and the operating conditions are the same for these two catalysts, whereas the pore radius of Pt/TiO_2-C is slightly smaller than that of Pt/C. Thus, the external mass transfer coefficients for Pt/TiO_2-C and Pt/C are the same, whereas the D_e for Pt/TiO_2-C is slightly smaller than that of Pt/C. In relating conversion to intrinsic rate constant, if the two catalysts have the same intrinsic activity (k_v), then the conversion for the Pt/TiO_2-C catalysts with smaller D_e will be lower than that for Pt/C. Because the Pt/TiO_2-C catalysts presented higher methanol conversion (Fig. 2), we can conclude that $k_{v(Pt/TiO_2\text{-}C)}$ is greater than $k_{v(Pt/C)}$. Moreover, the activity improvement assessed by use of $k_{o(Pt/TiO_2\text{-}C)}/k_{o(Pt/C)}$ will be underestimated, because $k_{v(Pt/TiO_2\text{-}C)}/k_{v(Pt/C)}$ is higher than $k_{o(Pt/TiO_2\text{-}C)}/k_{o(Pt/C)}$ due to the lower effective diffusivity of Pt/TiO_2-C, and also because the masking of the reaction by diffusion and mass transfer would make the difference in observed catalytic activity smaller.

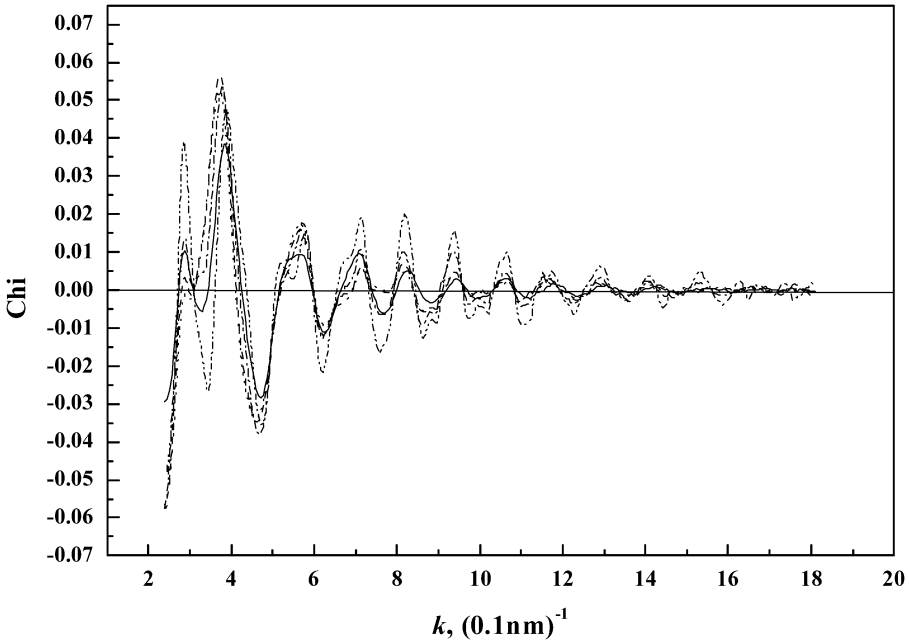

Fig. 3. Raw EXAFS data for fresh Pt/C catalyst (—), T130P5W6 (- - -), T160P10W6 (· · ·), T180P20W6 (- · - ·), and T220P40W6 (- ·· - ··).

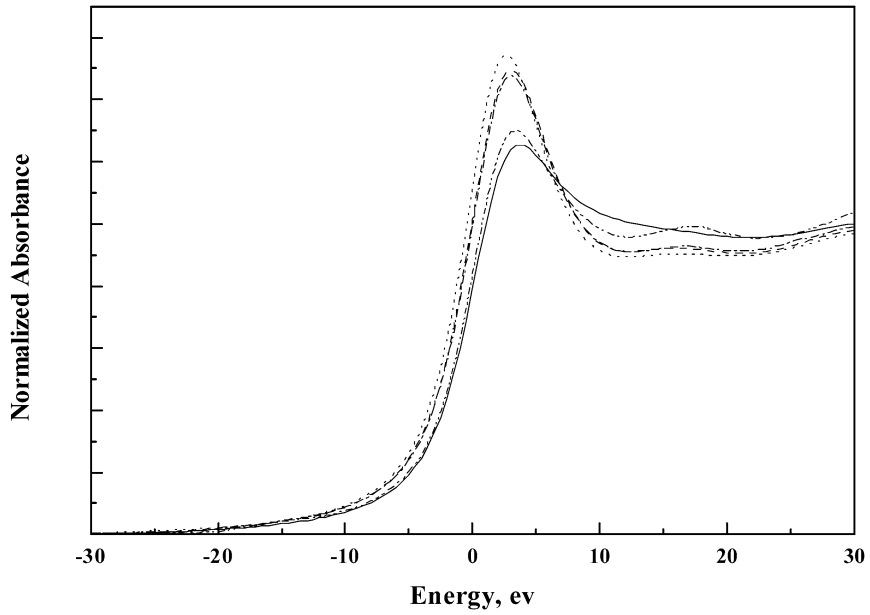

Fig. 4. Normalized Pt L_{III} absorption data for fresh Pt/C catalyst (—), T130P5W6 (- - -), T160P10W6 (· · ·), T180P20W6 (- · - ·), and T220P40W6 (- ·· - ··).

3.2. Structural characterization of Pt/C before and after reactions

A cubic spline background subtraction procedure was used to extract EXAFS oscillations from the experimental X-ray absorption data [22–24]. The resulting spectrum was divided by the edge jump step to obtain the final normalized EXAFS functions (Fig. 3) and the normalized Pt L_{III} absorption data (Fig. 4). For these raw EXAFS data, the signal-to-noise ratio was >30. (The noise amplitude was determined at $k \approx 14$ Å^{-1}, and the signal amplitude was determined at $k \approx 4$ Å^{-1}.)

Before the detailed EXAFS analysis, Fourier transforms were done to investigate the mechanism of catalyst deactivation based on the changes in morphology of the Pt clusters. A k^3-weighted Pt–Pt phase and an amplitude-corrected Fourier-transformed EXAFS function [23,24] over the range $4.0 < k < 14.0$ Å^{-1} for the fresh and used catalyst samples are shown in Fig. 5. The results demonstrate that the peaks corresponding to the first metal–metal shell (at about 2.8 Å) and higher shells (at about 3.9, 4.9, and 5.6 Å) are at the same positions and consistent with the nearest four neighbors in bulk face-centered cubic (fcc) Pt. The amplitude of peak at $R = 2.8$ Å for the used catalyst samples, T180P20W6 and T220P40W6, is larger than that for the fresh catalyst sample. Because the amplitude of the Fourier-transformed EXAFS function peaking at about

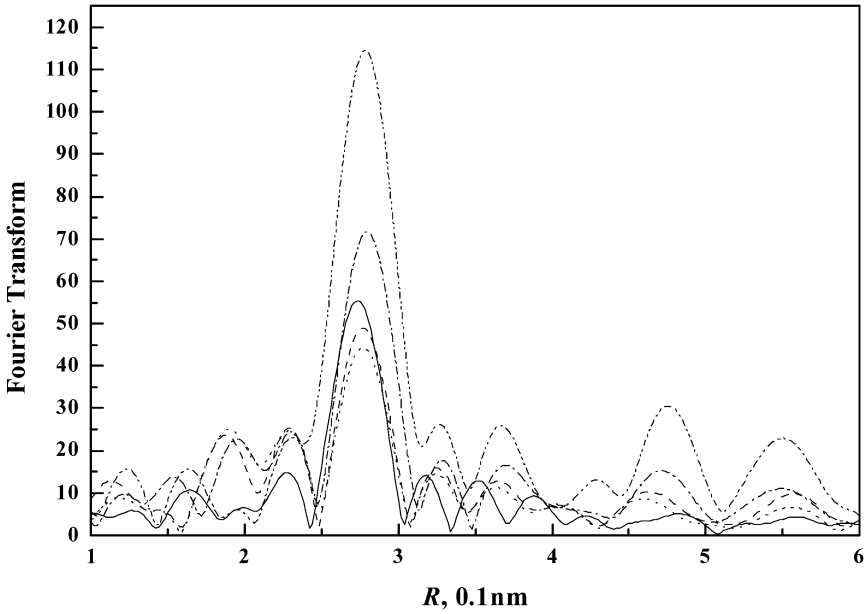

Fig. 5. Comparison of the magnitude of Fourier transforms (k^3-weighted, $\Delta k = 4.0$–14.0 Å^{-1}, Pt–Pt phase and amplitude corrected) of raw EXAFS data at Pt L_{III} edge between: fresh Pt/C catalyst (—), T130P5W6 (- - -), T160P10W6 (· · ·), T180P20W6 (- · - · -), and T220P40W6 (- · · - · ·).

2.8 Å reflects the metal particle size [22,25,26], the results indicate that Pt particles were agglomerated during the reaction at temperatures above 160 °C. Furthermore, the Pt particle size increased with elevating reaction temperatures. Because significant catalyst deactivation was also observed at reaction temperatures above 160 °C, the results suggest that metal aggregation is one factor in catalyst deactivation.

The X-ray absorption near-edge structure (XANES) results suggest that Pt was partially oxidized and existed in a high oxidation state. XANES intensity should decrease with increasing Pt particle size, as shown by Bazin et al. [27]. In contrast to this expectation, however, the experimental results showed that the metal-aggregated samples (T180P20W6 and T220P40W6) had a higher XANES intensity than the fresh catalyst (Figs. 4 and 5). These findings can be rationalized by the fact that the higher the oxidation state of the metal, the greater the probability of the transition and the higher the intensity of XANES [23]. Thus, we are tempted to conclude that Pt is partially oxidized in the WAO reaction.

The formation of platinum oxides during the reaction was further confirmed by detailed EXAFS analysis. A k^2-weighted Fourier transformation was performed on the EXAFS function over the range $3.0 < k < 14.5$ Å^{-1}. The major contributions were isolated by inverse Fourier transformation of the data in the range $1.15 < r < 3.25$ Å. At the beginning, the structural parameters characteristic of the Pt–Pt contribution were roughly determined by fitting the k^3-weighted Fourier-isolated EXAFS function in the range $6.0 < k < 14.0$ Å^{-1}, to deemphasize the low-Z contribution, Pt–O. An EXAFS function calculated from these parameters was then subtracted from the raw data (Fourier-isolated EXAFS function). The residual spectra were expected to represent the contributions from platinum–support interactions and/or platinum oxides. For the fresh Pt/C sample, the Pt–O phase-corrected Fourier transform of the residual spectra displayed a peak at about 2.2 Å (Fig. 6). The interaction between metal and surface oxygen on many metal oxides, such as MgO, Al_2O_3, and SiO_2, has been characterized with metal–support oxygen distances of 2.1 ± 0.1 Å (Pt–O_s) [28,29]. Based on these results, we inferred the peak at about 2.2 Å to be the contribution from Pt–O and/or Pt–C interactions (where O is the oxygen of carbon-containing functional groups and C is the carbon atoms of activated carbon) [30]. In contrast, for the used catalysts, a much shorter peak of about 2.05 Å emerged after Fourier transformation of the residual spectra (Fig. 6). The peak is consistent with the Pt–O bond distance of PtO_2 [31], suggesting that some of the Pt atoms were converted to platinum oxides. The structural parameters of both Pt–Pt and Pt–O were estimated by a nonlinear least squares multiple-shell fitting routine [22,32]; the results are given in Table 1. The decrease in average Pt–O bond distance combined with the increase in Pt–Pt coordination number indicate the formation of platinum oxides concomitant with the growth of Pt cluster at reaction temperatures above 160 °C.

3.3. Mechanism of Pt growth

Characteristic FTIR peaks of phenolic OH, carboxylate, ether, and epoxide appear in the range of 1000–1350 cm^{-1} [33]. The peaks at about 1600 and 1700 cm^{-1} are attributed to C=O and conjugated C=O vibrations, respectively [33]. As shown in Fig. 7a, the magnitude of the band in these regions underwent no significant changes at reaction temperatures below 160 °C, whereas it increased abruptly on further temperature elevations. Comparing the spectrum for catalysts after the WAO reaction run at 180 °C with that run at 160 °C reveals an additional peak at 3320 cm^{-1} (Fig. 7b). According to Nakanishi [34], this peak arises from an intermolecular hydrogen bond [33]. We thus suggest that partial oxidation occurs on the carbon

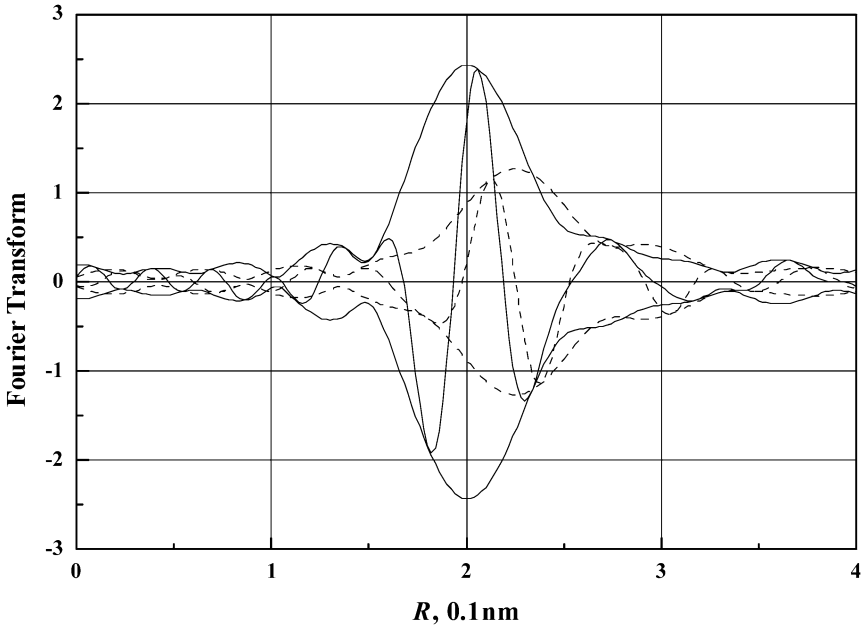

Fig. 6. Illustration of the EXAFS contributions characterizing platinum–support interaction and Pt–O contributions for the fresh catalyst (- - -) and T160P10W6 (—): magnitude and imaginary part of Fourier transform (k^3-weighted, Pt–O phase corrected, $\Delta k = 3.50$–10.0 Å^{-1}).

surface at a reaction temperature of 180 °C. Increasing the reaction temperature to 220 °C produced destruction of the catalyst. Moreover, the IR peak at 1421 cm^{-1} decreased sharply, the peaks in the ranges of 1000–1350 cm^{-1} and 2900–3500 cm^{-1} broadened, and strong broad peaks with shoulders appeared at 1590 cm^{-1} and 1400 cm^{-1} (Figs. 7b and 7c). Because the characteristic peak of carbonate species on metal oxides appears at 1300–1700 cm^{-1}, whereas that of simple carbonate appears at 1415 cm^{-1} [35], we suggest that a part of activated carbon was concomitantly combusted with the total oxidation of methanol. The broadened peaks at 1000–1350 cm^{-1} and 2900–3500 cm^{-1} may have resulted from the interactions between carbonate species and the functional groups on the carbon surface.

The FTIR results not only confirmed that activated carbon was oxidized concomitantly with the oxidation of methanol, but also indicated that the oxidation reaction is very sensitive to reaction temperature [14]. Combined with the growth of Pt clusters indicated by EXAFS, this can lead us to speculate the mechanism of Pt growth from the FTIR results. At a reaction temperature of 180 °C, the oxygen-containing groups may attract water molecules through H-bonding, which could reduce the affinity between Pt clusters and activated carbon, leading to migration of Pt clusters. Collisions between the mobile metal clusters offer the opportunity for agglomeration of metal clusters. At higher reaction temperatures, the mobility of Pt clusters was enhanced by the reaction of oxygen with carbon to form CO_2, leading to an agglomeration of Pt clusters. The adsorbed gases could lift the migrating Pt clusters, causing them to float over the carbon surface. This mechanism was proposed by Baker et al. [36], who found that Pd and Pt crystallites as large as 100 nm migrated at high temperatures in the presence of oxygen or hydrogen, leaving deep channels on the carbon surface.

In a typical oxidation reaction, a significant amount of reaction heat is generated. Notwithstanding the heat of reaction, which can be removed rapidly by the trickle-bed reaction system, the local heat generated from the exothermic reaction facilitates the inevitable catalytic combustion of activated carbon. In the reaction system, the surface properties of the catalysts will thus be altered by the oxidation of activated carbon itself, leading to change in metal–support affinities and morphology of Pt clusters.

3.4. Mechanism of Pt/C catalyst deactivation

It has been reported that oxidation of volatile organics catalyzed by noble metals undergoes the dissociative adsorption of oxygen first, followed by direct reaction of the dissociated oxygen with the reactant [37]. The reduced metallic Pt clusters are considered the active centers for catalytic oxidation [38]. As discussed above, Pt clusters grow under the WAO reaction conditions, leading to decreased Pt surface area and active centers. Thus, we are tempted to conclude that the Pt migration and Pt cluster growth are the main mechanisms of Pt/C catalyst deactivation. However, the formation of platinum oxides during the reactions, as evidenced by X-ray absorption spectroscopy, suggests that the oxidation-reduction mechanism [2,39] cannot be ruled out as a mechanism of Pt/C deactivation. The possible steps of this mechanism are as follows: (1) Methanol adsorbs on platinum and/or platinum oxides; (2) the adsorbed methanol reduces platinum oxides to platinum concomitantly with the formation of carbon dioxide and water; (3) platinum oxides are formed by the reaction of adsorbed oxygen with platinum; and (4) the adsorption strength of the adsorbed species may increase with the formation of metal oxides, and the reaction rate may be retarded by strong adsorption. Nikov and Paev have attributed the deactivation of Pd/alumina catalysts for glucose WAO to

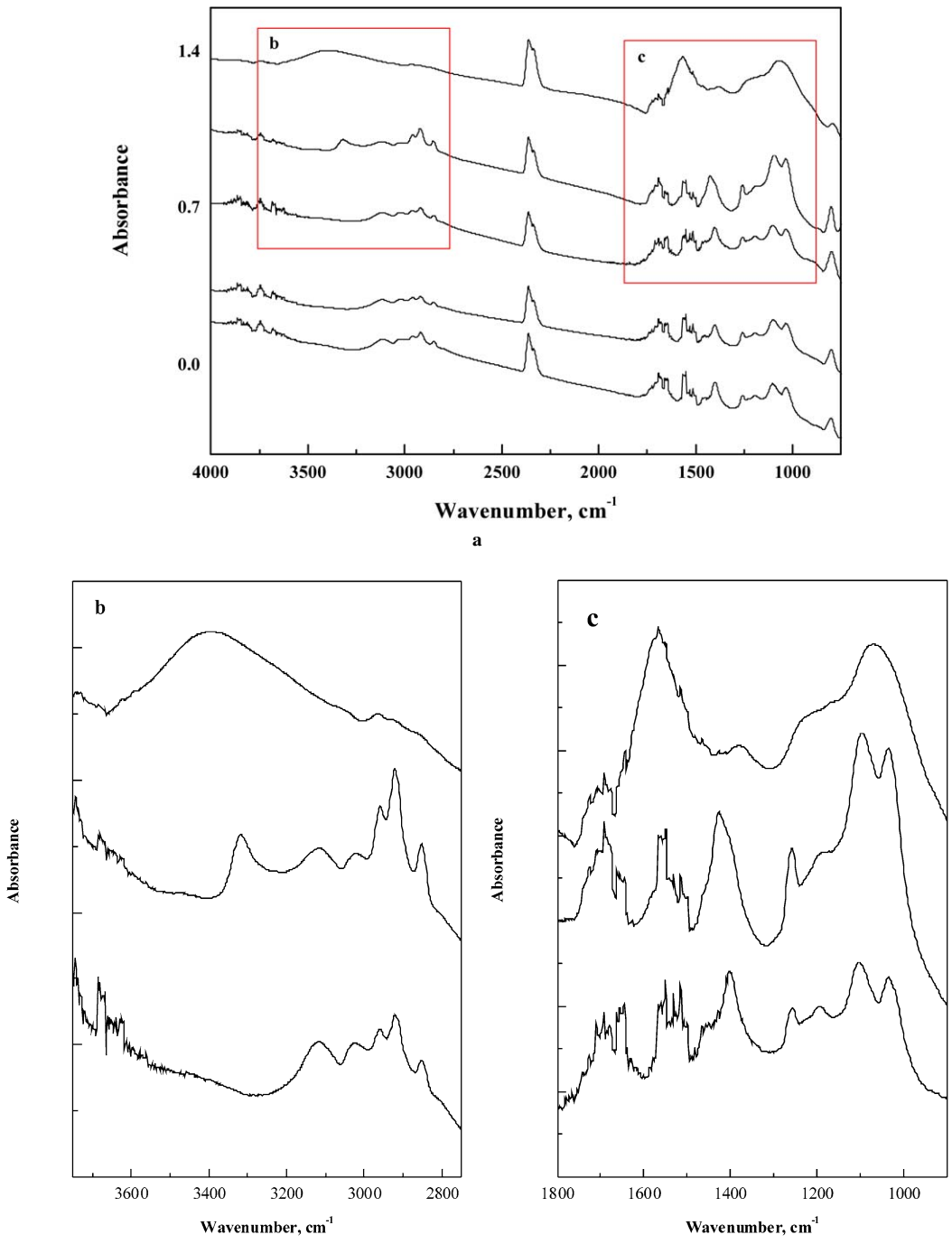

Fig. 7. (a) FT-IR spectrum characterizing fresh and used Pt/C catalysts (from bottom to top: fresh catalyst, T130P5W6, T160P10W6, T180P20W6, and T220P40W6); (b) magnifying the spectrum in the range between 2800 and 3600 cm^{-1}; (c) magnifying the spectrum in the range between 1000 and 1800 cm^{-1}.

the formation of PdO [40]. Our experimental results indicate that the effects of metal-oxide formation on catalyst deactivation were less pronounced than those of metal aggregation. As shown in Fig. 1 and Table 1, the deactivation rate for the reaction carried out at 160 °C was much lower than that run at 180 and 220 °C, whereas the EXAFS characterizing the used catalysts indicated that the used catalyst from the reaction run at 160 °C had the largest fraction of platinum oxide in the platinum clusters.

Metal leaching has also been identified as a factor in catalyst deactivation in WAO [2]. In the present study, the reaction products were specifically analyzed for metal using inductively coupled plasma–atomic emission spectroscopy. No platinum leaching from catalyst was detected, suggesting that any catalyst deactivation caused by metal leaching is insignificant.

3.5. Stable Pt/C for WAO and structural characterization of Pt/TiO_2-C

Pt interacts with Ti, leading to changes in the morphology of Pt clusters. As shown in Fig. 8, the amplitude of the major peak (at about 2.8 Å) for the Pt/TiO_2-C sample is lower than that

Table 1
Summary of EXAFS analysis results of Pt edge for Pt/C catalysts

Shell	N[a]	R[b] (Å)	$1000 \times \Delta\sigma^2$[c] (Å^2)	ΔE_0[d] (eV)	EXAFS reference
Fresh Pt/C CO/Pt = 0.52					
Pt–O	0.7 ± 0.1	2.16 ± 0.04	4 ± 2	−3 ± 4	Pt–O
Pt–Pt	6.4 ± 0.5	2.75 ± 0.01	5 ± 1	−1.0 ± 0.5	Pt–Pt
Variance:[e] k^0-weighted = 0.2, k^2-weighted = 0.2					
T130P5W6					
Pt–O	2.4 ± 0.1	2.03 ± 0.01	4 ± 1	3 ± 1	Pt–O
Pt–Pt	4.0 ± 0.3	2.76 ± 0.01	3 ± 1	−1.1 ± 0.5	Pt–Pt
Variance: k^0-weighted = 2.1, k^2-weighted = 3.9					
T160P10W6					
Pt–O	3.5 ± 0.1	2.03 ± 0.01	6 ± 1	3 ± 1	Pt–O
Pt–Pt	2.9 ± 0.3	2.76 ± 0.01	2 ± 1	0.2 ± 0.7	Pt–Pt
Variance: k^0-weighted = 0.3, k^2-weighted = 0.5					
T180P20W6					
Pt–O	2.6 ± 0.1	2.06 ± 0.01	4 ± 1	−2 ± 1	Pt–O
Pt–Pt	6.0 ± 0.3	2.77 ± 0.01	3.0 ± 0.3	−0.7 ± 0.3	Pt–Pt
Variance: k^0-weighted = 1.8, k^2-weighted = 1.9					
T220P40W6					
Pt–O	0.9 ± 0.1	2.10 ± 0.01	1 ± 1	−3 ± 1	Pt–O
Pt–Pt	10.8 ± 0.3	2.77 ± 0.01	2.9 ± 0.2	−1.9 ± 0.2	Pt–Pt
Variance: k^0-weighted = 0.9, k^2-weighted = 1.5					
T220P40W24					
Pt–O	0.5 ± 0.1	2.14 ± 0.02	−1 ± 2	−8 ± 4	Pt–O
Pt–Pt	10.6 ± 0.4	2.77 ± 0.01	3.5 ± 0.3	−0.8 ± 0.4	Pt–Pt
Variance: k^0-weighted = 1.8, k^2-weighted = 0.6					

[a] N, the coordination number for the absorber–backscattering pair.
[b] R, the average absorber–backscattering distance.
[c] $\Delta\sigma^2$, the difference in Debye–Waller factors between sample and standard.
[d] ΔE_0, the inner potential correction.
[e] Variance = $100 \times (\int (k^n(X_{\text{model}}(k) - X_{\text{exp}}(k))^2) / \int (k^n(X_{\text{exp}}(k))^2))$.

for Pt/C, indicating that adding TiO_2 retarded the growth of Pt clusters during catalyst preparation, and hence the Pt/TiO_2-C sample has higher initial activity. Furthermore, comparing the higher shells of the fresh Pt/C and Pt/TiO_2-C samples shows that all of the peak positions differ, indicating that the grafted TiO_2 alters the morphologies of the Pt clusters. The altered Pt morphology and improved stability maintenance during the reaction may be caused by the interactions between Pt clusters and TiO_2. Comparing the EXAFS spectra of Pt/TiO_2-C and TiO_2-C at the Ti edge shows an additional peak appearing at about 3.2 Å in the presence of Pt (Fig. 9a). Based on the model of the metal–support interaction in noble metal catalysts proposed by Mojet et al. [41], the small metal particles are in contact only with the oxide ions of the support. We suggest that the peak results from the interactions between the Pt cluster and the grafted TiO_2.

Fourier transform of the EXAFS characterizing the TiO_2-C sample exhibited a major peak at about 1.8 Å and a smaller peak at about 2.6 Å. Based on assignment of the EXAFS spectra characterizing the structure of TiO_2 incorporated within porous zeolite reported by Yamashita and Anpo [42], the major peak can be assigned to the neighboring atoms of Ti (Ti–O), and the smaller peak to the neighboring Ti atoms (Ti–Ti). Detailed EXAFS analysis showed that the TiO_2-C sample has an average Ti–O bond distance of 1.91 Å and an average coordination number of 4.1, indicating that most of TiO_2 species is in a tetrahedral structurel, whereas the presence of Ti–Ti with an average bond distance of 2.78 Å and a coordination number of 4.4 suggests formation of an aggregated TiO_2 species on the carbon surface (Table 2a).

The local structure of TiO_2 was further characterized by XANES at the Ti K edge. As shown in Fig. 9b, TiO_2-C showed

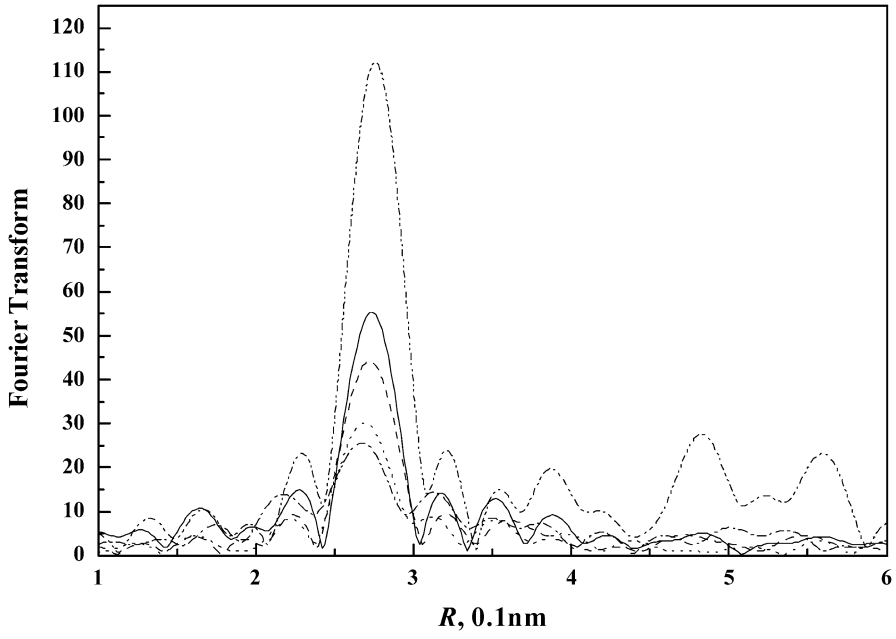

Fig. 8. Comparison of the magnitude of Fourier transforms (k^3-weighted, Δk = 4.0–14.0 Å^{-1}, Pt–Pt phase and amplitude corrected) of raw EXAFS data at Pt L_{III} edge between: fresh Pt/C catalyst (—), T220P40W24 (- ·· - ··), fresh Pt/TiO_2-C (···), T220P40W24(Pt/TiO_2-C) (- · - ·), and T220P40W24(Pt/TiO_2-C) after 300 °C hydrogen reduction (- - -).

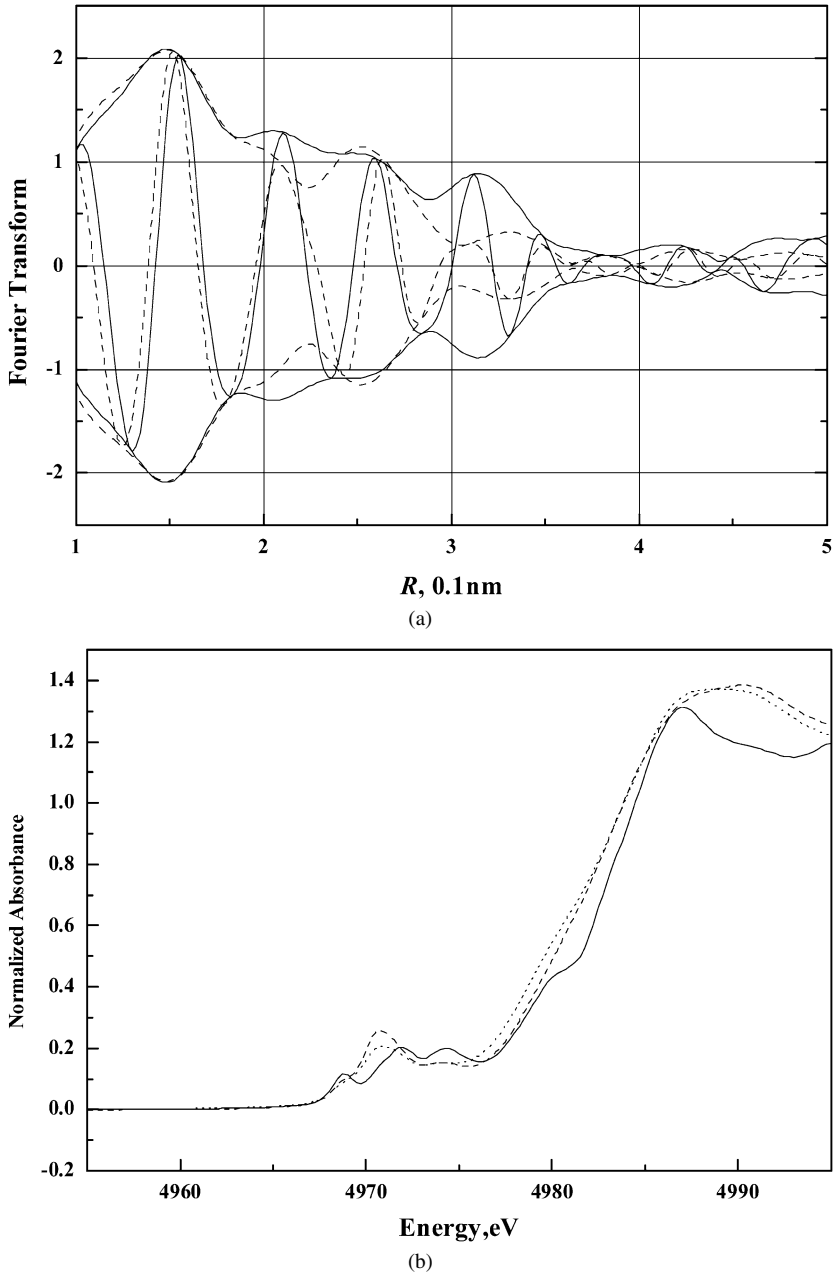

Fig. 9. (a) Comparison of the magnitude and imaginary of Fourier transforms (k^3-weighted, $\Delta k = 4.0$–12.0 Å^{-1}) of raw EXAFS data at Ti K edge between: TiO_2-C support (- - -), fresh Pt/TiO_2-C catalyst (—). (b) Comparison of Ti K edge spectra of anatase (—), TiO_2-C support (- - -), fresh Pt/TiO_2-C catalyst (···).

a clear pre-edge absorption peak at 4971 eV and two rather small shoulders at 4968 and 4973 eV, respectively. These findings differ from those for anatase, which showed three low-intensity pre-edge peaks and one shoulder at the edge jump. It is generally accepted that pre-edge spectrum at Ti K edge reveals the symmetry of TiO_2 [43]. Octahedral symmetry of Ti(IV)–A_{1g}–T_{2g} or A_{1g}–E_g are symmetry (Laporte)-forbidden and of lower intensity, whereas tetrahedral symmetry of the A_1–T_2 transition is allowed and intensive. Hence, combining EXAFS and XANES results, we suggest that most aggregated TiO_2 species are monolayer and have a tetrahedral coordination, whereas a small amount of TiO_2 is in a structure resembling anatase with an octahedral coordination. Based on the structure of TiO_2 estimated by EXAFS, at least 1.8 g of TiO_2 per gram of carbon is needed to completely cover the carbon surface with a monolayer of TiO_2, which is far more than that used for the preparation of TiO_2-C in this study.

Pt clusters were anchored on the polymeric TiO_2, as evidenced by the Ti–Pt contributions. The EXAFS contribution from the Pt–TiO_2 interaction was estimated by the difference file technique [32]. The structural parameters of Ti–O and Ti–Ti contributions were first estimated by calculating the EXAFS functions that agree as closely as possible with the experimental EXAFS results of Pt/TiO_2-C in r space ranging from 1.0 to 3.5 Å. EXAFS functions of Ti–O and Ti–Ti were calculated from the estimated structural parameters, and the residual spectrum was expected to include the Ti–Pt contribution. A symmetric peak appeared at about 3.2 Å after Ti–Pt phase-

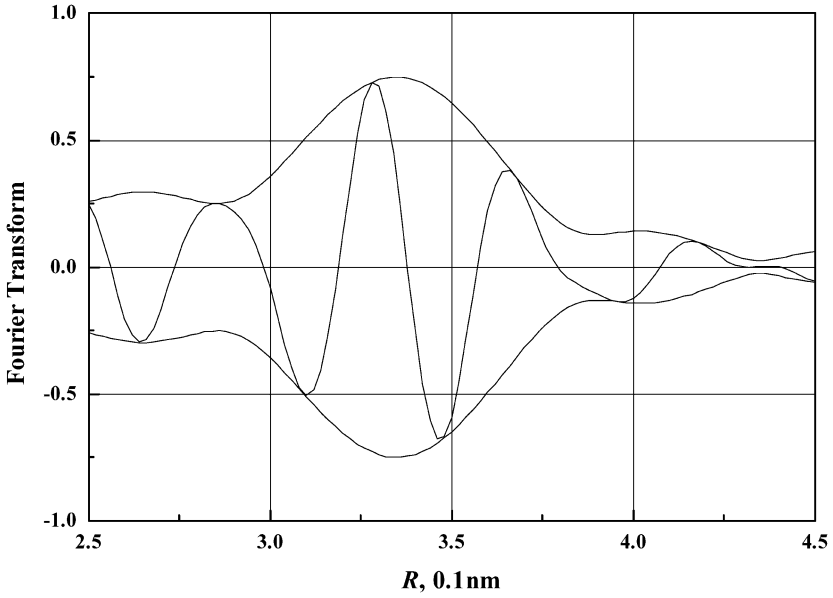

Fig. 10. Illustration of the EXAFS contributions characterizing Pt–TiO_2 interactions for the Pt/TiO_2-C catalyst: magnitude and imaginary part of Fourier transform (k^3-weighted, Ti–Pt phase corrected, $\Delta k = 4.0$–12.0 Å^{-1}).

corrected Fourier transform was performed on the residual spectrum (Fig. 10). For an X–Y absorber–backscattering pair, peak, which has a positive imaginary part of the phase-corrected EXAFS function, are due to neighbors of type Y [44]. These results confirm that Pt is the backscattering atom and indicate that Pt clusters are anchored on the aggregated TiO_2.

Detailed EXAFS analysis at the Pt edge for Pt/TiO_2-C yielded findings similar to those for Pt/C except that the Pt–Ti contribution was considered. Hence, after subtracting Pt–Pt contributions from the raw data, the residual spectrum was expected to represent the interactions between Pt clusters and the aggregated TiO_2 including Pt–$O_{support}$ and Pt–Ti. The structural parameters of Pt–Pt, Pt–O, and Pt–Ti were thus estimated by a nonlinear least squares multiple-shell fitting routine; the results are summarized in Table 2b.

3.6. EXAFS characterization of structural changes in fresh and used Pt/C and Pt/TiO_2-C catalysts

In the WAO aging test, the Pt clusters on the Pt/C were induced to migrate and aggregate, leading to decreased catalytic activity (Table 1, Fig. 1). Specifically, the average Pt–Pt bond distance increased from 2.75 to 2.77 Å, and the coordination number increased from 6.4 to 10.8. In contrast, as shown in Fig. 8, agglomeration of Pt clusters was less pronounced for the Pt/TiO_2-C sample after the WAO test reaction. Because the Pt clusters on Pt/TiO_2-C might be oxidized partially, estimating the Pt cluster size of such a partially oxidized sample directly based on the EXAFS results is rather difficult. Hence, the used catalyst sample was reduced in flowing H_2 at 300 °C, and the structure was characterized by EXAFS. The Pt–Pt coordination number of 5.4 is only slightly larger than that of the fresh Pt/TiO_2-C catalyst, indicating that migration of Pt clusters during the WAO reaction and reduction was greatly inhibited by the use of TiO_2-C supports.

Table 2
(a) Summary of EXAFS analysis results of Ti edge for TiO_2-C support and Pt/TiO_2-C catalysts. (b) Summary of EXAFS analysis results of Pt edge for Pt/TiO_2-C catalysts

Shell	N[a]	R[b] (Å)	$1000 \times \Delta\sigma^2$[c] (Å^2)	ΔE_0[d] (eV)	EXAFS reference
		(a)			
TiO_2-C					
Ti–O	4.1 ± 0.4	1.91 ± 0.01	4 ± 2	0.8 ± 0.9	Ti–O
Ti–Ti	4.4 ± 0.9	2.78 ± 0.02	9 ± 4	5 ± 2	Ti–Ti
Variance:[e] k^0-weighted = 0.4, k^2-weighted = 0.6					
Pt/TiO_2-C					
Ti–O	4.4 ± 0.4	1.95 ± 0.01	4 ± 2	1 ± 1	Ti–O
Ti–Ti	4.1 ± 1.0	2.77 ± 0.02	5 ± 4	-8 ± 2	Ti–Ti
Ti–Pt	0.5 ± 0.2	3.23 ± 0.04	3 ± 2	3 ± 2	Ti–Pt
Variance: k^0-weighted = 0.4, k^2-weighted = 0.7					
		(b)			
Fresh Pt/TiO_2-C CO/Pt = 0.88					
Pt–O	0.8 ± 0.4	2.19 ± 0.05	5 ± 7	-13 ± 4	Pt–O
Pt–Pt	4.3 ± 0.8	2.72 ± 0.02	5 ± 2	-1 ± 1	Pt–Pt
Pt–Ti	1.5 ± 0.6	3.17 ± 0.06	9 ± 6	8 ± 5	Pt–Ti
Variance: k^0-weighted = 0.5, k^2-weighted = 0.6					
T220P40W24(Pt/TiO_2-C)					
Pt–O	1.2 ± 0.3	2.16 ± 0.05	1 ± 5	-12 ± 4	Pt–O
Pt–Pt	3.7 ± 0.9	2.70 ± 0.03	7 ± 9	-2 ± 3	Pt–Pt
Pt–Ti	1.0 ± 0.6	3.16 ± 0.05	-7 ± 3	8 ± 3	Pt–Ti
Variance: k^0-weighted = 0.7, k^2-weighted = 1.6					
Hydrogen regenerated T220P40W24(Pt/TiO_2-C) CO/Pt = 0.76					
Pt–O	0.5 ± 0.3	2.18 ± 0.04	-1 ± 8	-14 ± 8	Pt–O
Pt–Pt	5.4 ± 0.9	2.73 ± 0.02	2 ± 3	5 ± 3	Pt–Pt
Pt–Ti	1.4 ± 0.6	3.28 ± 0.06	10 ± 6	-4 ± 4	Pt–Ti
Variance: k^0-weighted = 0.3, k^2-weighted = 0.5					

[a] N, the coordination number for the absorber–backscattering pair.
[b] R, the average absorber–backscattering distance.
[c] $\Delta\sigma^2$, the difference in Debye–Waller factors between sample and standard.
[d] ΔE_0, the inner potential correction.
[e] Variance = $100 \times (\int (k^n(X_{\text{model}}(k) - X_{\text{exp}}(k))^2) / \int (k^n(X_{\text{exp}}(k))^2))$.

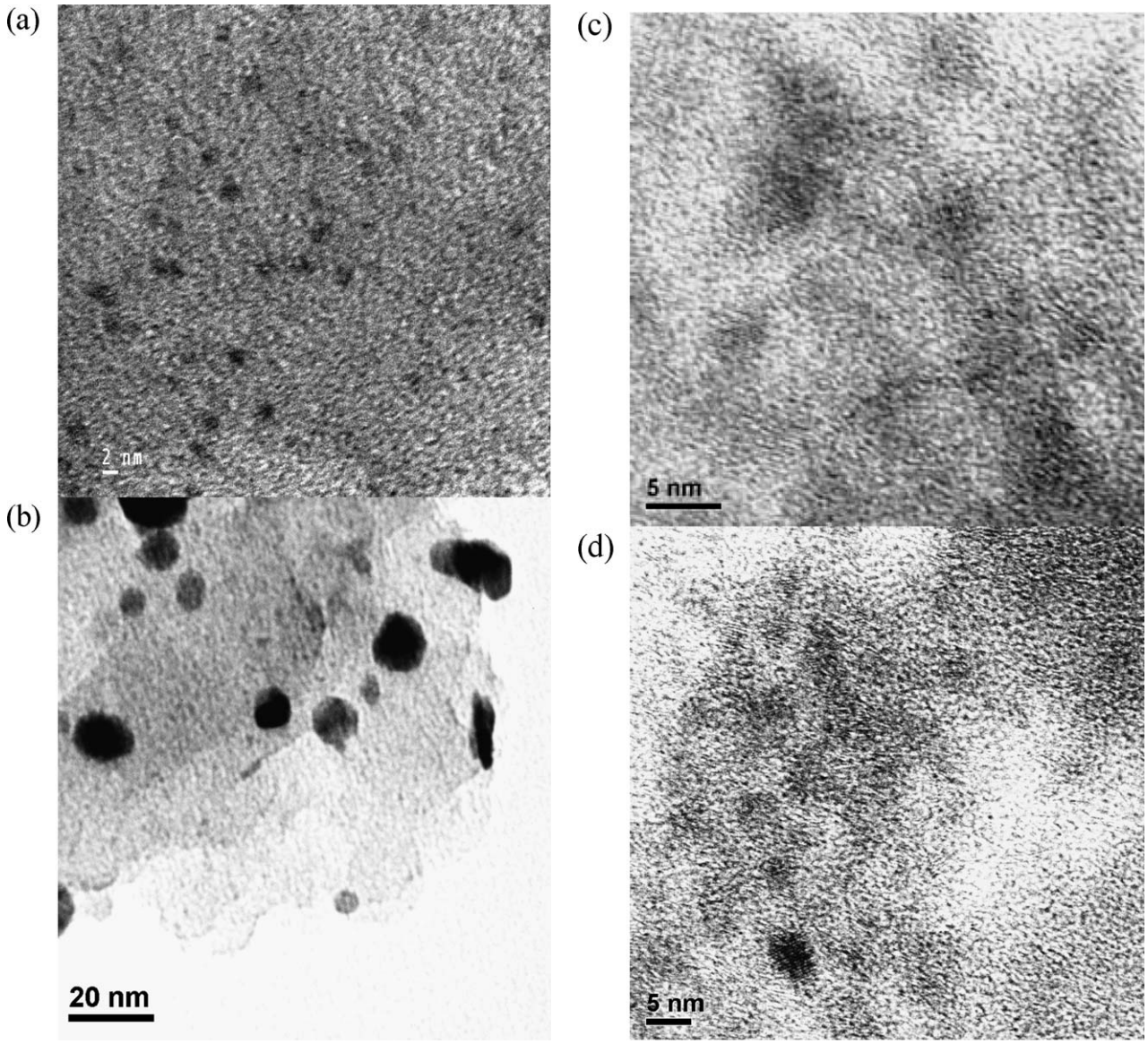

Fig. 11. TEM photographs of (a) fresh Pt/C; (b) T220P40W24; (c) fresh Pt/TiO_2-C; (d) T220P40W24(Pt/TiO_2-C).

3.7. Mechanisms of stabilization: Pt anchoring

The role of grafted TiO_2 in inhibiting Pt migration during H_2 reduction and WAO was further confirmed by TEM and CO chemisorption. Pt clusters from different regions were measured; the TEM micrographs, representing the cluster size distribution, are shown in Fig. 11. For the Pt/C catalyst, the average Pt cluster size increased from about 2 to 10 nm, whereas for both the fresh and used Pt/TiO_2-C catalyst, the Pt clusters appeared to be <1 nm. Because distinguishing the particle sizes of Pt and TiO_2 is difficult using TEM, Pt dispersion was further determined using CO chemisorption. The results show that using grafted TiO_2 increased Pt dispersion by 70% (Tables 1 and 2). Pt/TiO_2–Al_2O_3 catalyst was prepared and fully characterized by Resende et al. [18], who reported that the dispersion of Pt on TiO_2-grafted Al_2O_3 support was higher than that on Al_2O_3 alone. Our TEM and CO chemisorption results are consistent with those of Resende et al. [18]. Moreover, EXAFS results further indicate that Pt clusters on TiO_2-C were anchored on the polymeric TiO_2 and exhibited much higher stability than those on activated carbon. The catalytic performance results, combined with structural information obtained from EXAFS and TEM spectroscopy, provide a basis for the greatly improved catalyst stability achieved by modifying the carbon supports with grafted TiO_2. Apparently, the grafted TiO_2 anchors Pt and maintains it in small ensembles, thereby maintaining catalyst activity.

It has been claimed in a patent that the CO tolerance and stability of carbon-supported Pt or Pt–Ru catalyst used in fuel cells can be increased by the addition of TiO_2 [45]. The reason for this improved catalytic performance is unclear, although we suspect that anchoring of Pt by grafted TiO_2 may play an important role. Moreover, it has been reported in the literature that strong metal–support interactions induced by high-temperature reduction may alter the phase of active sites, resulting in a change in catalytic properties [46,47]. Hence, further studies on

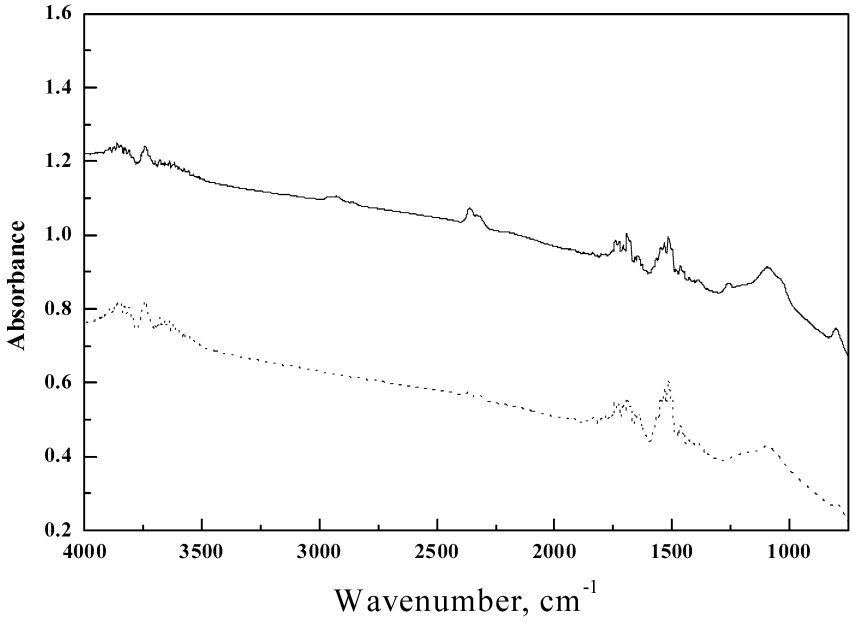

Fig. 12. FT-IR spectrum characterizing fresh and used Pt/TiO_2-C catalysts: fresh catalyst (- - -), T220P40W24(Pt/TiO_2-C) (—).

grafted TiO_2 and the effects of treatment temperature on strong metal–support interactions could be interesting topics in fuel cell research.

3.8. Other possible mechanisms

Because Pt clusters were anchored on the grafted TiO_2, we might expect that grafted TiO_2 acts as an insulator to minimize the catalytic combustion of carbon by keeping Pt clusters from direct contact with carbon support. However, as shown in Fig. 12, the peaks characterizing oxygen-containing functional groups on activated carbon increased after aging test reactions, indicating that carbon is burned, contrary to our initial expectation. Those results thus suggest that although this mechanism might not be ruled out, anchoring of Pt on TiO_2 to maintain it in small clusters during WAO is the main reason for the improved catalyst stability.

4. Conclusion

Activated carbon-supported platinum catalysts, Pt/C, have high activity and selectivity for WAO. However, its stability is very sensitive to the reaction temperature. At a reaction temperature of 180 °C or higher, the catalyst deactivated rapidly immediately after the start of the run. Based on characterization of the fresh and used catalysts by FTIR, EXAFS, CO chemisorption, and TEM, the rapid catalyst deactivation at high temperatures was determined to result from Pt migration and agglomeration, resulting from catalytic combustion of carbon supports. From an industrial application standpoint, it is most crucial to develop catalysts that maintain high activity for long-term operation. Hence the performance of the Pt/C catalyst was improved by grafting TiO_2 onto the carbon support. The TiO_2 on the carbon was found to be an excellent anchor for the Pt. By anchoring Pt on TiO_2, Pt clusters were kept small, and a high level of catalyst activity was maintained during the extended reaction period.

Acknowledgments

The EXAFS data were analyzed using the FEFF and XDAP data analysis programs, and reference files were provided by Dr. B.C. Gates. This research was supported by the National Science Council of the Republic of China (contracts NSC 93-2214-E-194-009 and NSC 93-2120-M-194-002). The authors are grateful to the X-ray beam staff of NSRRC, the Taiwan light source (TLS), for their assistance.

References

[1] V.S. Mishra, V.V. Mahajani, J.B. Joshi, Ind. Eng. Chem. Res. 34 (1995) 2.
[2] J. Levec, A. Pintar, Catal. Today 24 (1995) 51.
[3] F. Luck, Catal. Today 27 (1996) 195.
[4] F. Luck, Catal. Today 53 (1999) 81.
[5] S. Imamura, Ind. Eng. Chem. Res. 38 (1999) 1743.
[6] C.-C. Hsieh, J.-F. Lee, Y.-R. Liu, J.-R. Chang, Waste Manage. 22 (2002) 739.
[7] E. Auer, A. Freund, J. Pietsch, T. Tacke, Appl. Catal. A 173 (1998) 259.
[8] T.Y. Yan, Wastewater Treatment by Catalytic Oxidation, US Patent 5,338,463 (1994).
[9] P. Gallezot, S. Chaumet, A. Perrard, P. Isnard, J. Catal. 168 (1997) 104.
[10] H.T. Gomes, J.L. Figueiredo, J.L. Faria, Appl. Catal. B 27 (2000) L217.
[11] J. Trawczyński, Carbon 41 (2003) 1515.
[12] A. Fortuny, J. Font, A. Fabregat, Appl. Catal. B 19 (1998) 165.
[13] A. Fortuny, C. Miro, J. Font, A. Fabregat, Catal. Today 48 (1998) 323.
[14] E. Sabio, E. González, J.F. González, C.M. González-García, A. Ramiro, J. Gañan, Carbon 42 (2004) 2285.
[15] B. Tryba, A.W. Morawski, M. Inagaki, Appl. Catal. B: Environ. 41 (2003) 427.
[16] S. Srinivasan, A.K. Datye, M.H. Smith, C.H.F. Peden, J. Catal. 145 (1994) 563.
[17] H.-M. Lin, S.-T. Kao, K.-M. Lin, J.-R. Chang, S.-G. Shyu, J. Catal. 224 (2004) 156.
[18] N.S. de Resende, J.-G. Eon, M. Schmal, J. Catal. 183 (1999) 6.

[19] N. Macleod, R. Cropley, J.M. Keel, R.M. Lambert, J. Catal. 221 (2004) 20.
[20] S. Cheng, K.T. Chuang, Can. J. Chem. Eng. 70 (1992) 727.
[21] R. Aris, in: G.F. Froment, K.B. Bischoff (Eds.), Chemical Reactor Analysis and Design, Wiley, New York, 1990, p. 171.
[22] J.B.A.D. Van Zon, Ph.D. Dissertation, Eindhoven Univ. Technology, The Netherlands, 1988.
[23] D.C. Koningsberger, R. Prins, X-Ray Absorption: Principles, Applications, Techniques of EXAFS, SEXAFS, and XANES, Wiley, New York, 1988.
[24] K. Asakura, in: Y. Iwasawa (Ed.), X-Ray Absorption Fine Structure for Catalysts and Surface, World Scientific, Singapore, 1995, p. 33.
[25] S.K. Purnell, K.M. Sanchez, R. Patrini, J.-R. Chang, B.C. Gates, J. Phys. Chem. 98 (1994) 1205.
[26] G.H. Via, J.H. Sinfelt, F.W.J. Lytle, Chem. Phys. 68 (1978) 2009.
[27] D. Bazin, D. Sayers, J. Rher, J. Phys. Chem. B 101 (1997) 11040.
[28] D.C. Koningsberger, B.C. Gates, Catal. Lett. 14 (1992) 271.
[29] K. Asakura, H. Nagahiro, N. Ichikuni, Y. Iwasawa, Appl. Catal. A 188 (1999) 313.
[30] C.-C. Shih, J.-R. Chang, Mater. Chem. Phys. 92 (2005) 89.
[31] Inorganic Crystal Structure Database (ICSD for WWW).
[32] M. Varrkamp, XDAP User's Guide, XAFS Services International, The Netherlands, 1996.
[33] V. Gómez-Serrano, F. Piriz-Almeida, C.J. Durán-Valle, J. Pastor-Villegas, Carbon 37 (1999) 1517.
[34] K. Nakanishi, Infrared Absorption Spectroscopy-Practical, Holden-Day, San Francisco, CA, 1962, p. 30.
[35] L.H. Little, A.V. Kiselev, V.I. Lygin, Infrared Spectra of Adsorbed Species, Academic Press, New York, 1966, pp. 77–84.
[36] R.T.K. Baker, Stability of Supported Catalysts: Sintering and Redispersion, Catalytic Studies Division, CA, 1991, p. 84.
[37] J.J. Spivey, Ind. Eng. Chem. Res. 26 (1987) 2165.
[38] J. Völter, G. Lietz, H. Spindler, H. Lieske, J. Catal. 104 (1987) 375.
[39] G. Baldi, S. Goto, C.-K. Chow, J.M. Smith, Ind. Eng. Chem., Process Des. Dev. 13 (1974) 447.
[40] I. Nikov, K. Paev, Catal. Today 24 (1995) 41.
[41] B.L. Mojet, J.T. Miller, D.E. Ramaker, D.C. Koningsberger, J. Catal. 186 (1999) 373.
[42] H. Yamashita, M. Anpo, Curr. Opin. Solid State Mater. Sci. 7 (2003) 471.
[43] Z. Liu, R.J. Davis, J. Phys. Chem. 98 (1994) 1253.
[44] P.A. Lee, G. Beni, Phys. Rev. B 15 (1977) 2862.
[45] H. Yang, C.-P. Liu, T.-H. Lu, Y.-W. Tang, Fuel Cell Anode Catalyst Production, Chinese Patent CN 1,280,398 (2001).
[46] F.B. Noronha, C.A. Perez, M. Schmal, R. Fréty, Phys. Chem. Chem. Phys. 1 (1999) 2861.
[47] S.J. Tauster, S.C. Fung, J. Catal. 122 (1990) 211.